Dynamics of a bacterial flagellum under reverse rotation

Tapan Chandra Adhyapak*a and Holger Starka

To initiate tumbling of an *E. coli*, one of the helical flagella reverses its sense of rotation. It then transforms from its normal form first to the transient semicoiled state and subsequently to the curly-I state. The dynamics of polymorphism is effectively modeled by describing flagellar elasticity through an extended Kirchhoff free energy. However, the complete landscape of the free energy remains undetermined because the ground state energies of the polymorphic forms are not known. We investigate how variations in these ground state energies affect the dynamics of a reversely rotated flagellum of a swimming bacterium. We find that the flagellum exhibits a number of distinct dynamical states and comprehensively summarize them in a state diagram. As a result, we conclude that tuning the landscape of the extended Kirchhoff free energy alone cannot generate the intermediate full-length semicoiled state. However, our model suggests an ad hoc method to realize the sequence of polymorphic states as observed for a real bacterium. Since the elastic properties of bacterial flagella are similar, our findings can easily be extended to other peritrichous bacteria.

1 Introduction

Although much research has been performed on the mechanical properties of a prokaryotic or bacterial flagellum and how these properties are related to the overall bacterial dynamics ^{1–16}, still our understanding of the complex aspects of bacterial locomotion, such as tumbling of an *E. coli*, remains incomplete ^{14,17–19}. The locomotion of bacteria involves rich and complex physics ^{20–29}. In addition, experiments on the collective behavior of bacteria have opened new directions of physics per se, demonstrating ground-breaking phenomena such as turbulence and superfluidity in living systems ^{30–33}. A comprehensive knowledge of bacterial locomotion is also necessary for a complete understanding of these novel phenomena.

One main challenge in dealing with the mechanics of the bacterial flagellum is still to gain a full theoretical understanding of the polymorphic transformations shown by the flagellum during tumbling ^{2,17}. The flagellum can exist in different stable polymorphic forms, transitions among which are induced mechanically, either by the reverse rotation of the flagellum ^{14,17,18}, by the application of stretching forces ^{3,12}, or by external flows ^{7,34}. Rotation induced polymorphic transitions occur during the locomotion of the bacterium and affect the overall bacterial dynamics ¹⁷. An *E. coli* flagellum, for example, usually stays in the normal form; but under reverse rotation, it transforms first into the semicoiled state, and then fully assumes the curly-I state ³⁵.

A number of approaches using the Kirchhoff free energy density

and extended versions of it, were proposed to deal with the flagellar multistability 6-8,12. In Ref. 14 an extended Kirchhoff free energy successfully generates the rotation-induced polymorphic transformations during the locomotion of the bacterium ¹⁴. However, the landscape of this free energy with the fixed positions of the local minima and the harmonic shape in their neighborhood was not fully explored. Using a linear increase in the ground state energies of the local minima, the authors were able to demonstrate an E. coli flagellum transforming from the normal to the curly-I form. However, the transient semicoiled form in between was not observed. In our study here, we explore the flagellar dynamics in the full free energy landscape by studying the impact of the ground state energies. Changes in their values affect the heights of the transition barriers between the local minima 6,8,12 , which the flagellum has to pass to locally transform from one polymorphic state to the other. Thus the full landscape of the free energy determines the flagellar dynamics during reverse rotation including possible transient and final steady states.

In this paper we present a systematic study of how variations in the unknown local ground state energies affect the dynamics of a reversely rotated flagellum attached to a cell body. We study the nature of transitions and the dynamic stability of polymorphic forms as a function of the barrier heights and arrive at a comprehensive state diagram that classifies different scenarios of flagellar dynamics in the parameter space. In particular, we show that at the level of the present formulation of flagellar mechanics the experimentally observed transient semicoiled state, intermediate in the sequence of polymorphic states during tumbling, cannot be reproduced. However, we suggest an alternative way within our

^a Institut für Theoretische Physik, Technische Universität Berlin, Hardenbergstrasse 36, 10623 Berlin, Germany. E-mail: tapan.c.adhyapak@tu-berlin.de

model to realize the desired sequence of transitions.

In the following we first outline in sec. 2 the observations on a reversely rotated flagellum and introduce the extended Kirchhoff elastic free energy. Section 3 summarizes the equations of motion of the bacterium and their numerical implementation. Results are then presented in sec. 4, followed by a discussion and conclusions in secs. 5 and 6, respectively.

2 Flagellar conformations during reversal and appropriate modeling

The reversal of rotating flagella during locomotion has been most elaborately studied for $E.\ coli^{2,18,35}$. So, in our study we take $E.\ coli$ as the prototype for flagellated bacteria. However, since prokaryotic flagella of peritrichous bacteria have a common molecular structure, which ultimately determines their elasticity 36,37 , we expect our results to be valid for a wide range of bacteria.

An E. coli has several flagella, which act as propelling units for the bacterium ³⁵. The flagellum is a passive helical filament, connected at one end to a rotary motor embedded in the cell wall. Most of the time the motor rotates the flagellum in the counterclockwise sense (as viewed along the flagellum from its free end toward the cell body) generating the thrust force for propelling the bacterium. At this stage the flagellum assumes the normal form, a left-handed helix of known radius and pitch. It forms a bundle with other flagella and thereby defines a unique direction for the net propulsive force. Frequently, however, the motor reverses and rotates the flagellum clockwise. This forces the bundle to disrupt and the cell body to tumble. A sequence of polymorphic transitions in the flagellum is observed ^{2,18}. In each case these transitions start at the cell body and proceed towards the free flagellar end. The whole flagellum thus changes from the normal state, first to the right-handed semicoiled form, and then finally to the right-handed curly-I form [see Figs. 1(b) and (d)].

An understanding of the polymorphic states was developed based on the molecular structure of the flagellum ^{37–39}. Following this bottom-up approach, several models describe the dynamics of polymorphism by coarse-graining over the molecular scale ^{40–42}. However, an alternative approach, where Kirchhoff's continuum theory of an elastic rod was extended to incorporate multistability, turns out to be simpler and more effective ^{6,7,43}. One example of such an extended Kirchhoff free energy reproduces stretching induced polymorphism most accurately as demonstrated in Ref. 12 and is also appropriate for modeling rotation-induced polymorphism in a moving bacterium ¹⁴. We now describe it in more detail.

2.1 Flagellar elasticity: extended Kirchhoff elastic free energy

We treat the flagellum as a slender body and parametrize its centerline $\mathbf{r}(s)$ by the contour length s^{12} . The conformation of a distorted flagellum including twist deformations is characterized by orthonormal material tripods $\{\mathbf{e}_1(s), \mathbf{e}_2(s), \mathbf{e}_3(s)\}$ at each point on the centerline, where \mathbf{e}_3 is the local tangent to the centerline at s and unit vectors \mathbf{e}_1 and \mathbf{e}_2 point along the principal axes of

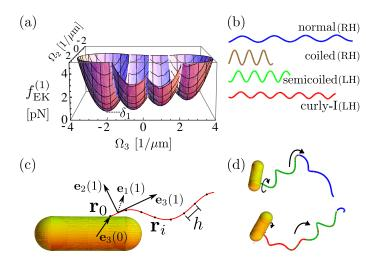


Fig. 1 (a) The first term of the extended Kirchhoff free energy density, $f_{\rm EK}^{(1)}$, plotted against Ω_2 and Ω_3 for $\Omega_1=0$. The local minimum of the normal form with ground state energy δ_1 is shown. The true local minima for the coiled, semicoiled, and curly-I forms are situated at $\Omega_1 \neq 0$. (b) Planar projections of four helical polymorphic forms of a filament with a fixed contour length: normal (blue), coiled (brown), semicoiled (green), and curly-I (red). (c) A schematic of the model bacterium used in our simulations. The cell body and part of the discrete flagellum with a discretization length h (drawn out of proportion) are shown. Other components are as described in the text. (d) Two snapshots from our simulations with a CW rotated flagellum: (top) a growing semicoiled domain (green) evades the normal state (blue) and (bottom) a growing curly-I domain (red) evades the semicoiled state (green).

the flagellar cross section. The rotational strain vector Ω in

$$\partial_s \mathbf{e}_{\nu} = \Omega \times \mathbf{e}_{\nu},\tag{1}$$

with v=1,2,3, transports the material tripod along the centerline. Therefore, together with the position $\mathbf{r}(s=0)$ of one flagellar end, $\Omega(s,t)$ carries the complete information for the conformation of the flagellum at time t. Conversely, given the conformation in terms of the centerline $\mathbf{r}(s)$ and the material tripods at each s, the rotational strain vector Ω can be worked out from Eq. (1). Introducing the angle α between \mathbf{e}_1 and the local normal to the centerline, $\mathbf{n} \propto \partial_s^2 \mathbf{r}(s)$, one can relate the components Ω_1, Ω_2 and Ω_3 of Ω with respect to the local material frame to the curvature κ and torsion τ of the flagellum 12:

$$\Omega_1 = \kappa \sin \alpha, \quad \Omega_2 = \kappa \cos \alpha, \quad \Omega_3 = \tau + \partial_s \alpha.$$
(2)

In harmonic approximation, the energy required per unit length of the flagellum to induce small deformations $d\Omega = \Omega - \Omega^{(n)}$ from the stable ground state $\Omega^{(n)}$, is the Kirchhoff elastic free energy density ⁴⁴,

$$f_{K}(\Omega, \Omega^{(n)}) = \frac{A}{2} \left[(d\Omega_{1})^{2} + (d\Omega_{2})^{2} \right] + \frac{C}{2} (d\Omega_{3})^{2},$$
 (3)

where A and C are the respective bending and twist rigidities of the flagellum, assuming a circular cross section. Assigning $f_{\rm K}(\Omega,\Omega^{(n)})$ and a ground state energy δ_n to each polymorphic form $\Omega^{(n)}$, an extended version of the Kirchhoff free energy density, capable of describing the multistability of a flagellum, is for-

mulated as 14

$$f_{\text{EK}} = \min_{\forall n} \left[f_{\text{K}}(\Omega, \Omega^{(n)}) + \delta_n \right] + \frac{A}{2} \xi^2 (\partial_s \Omega)^2. \tag{4}$$

Here, $\Omega^{(n)}$, n = 1-4, correspond, respectively, to the normal, coiled, semicoiled, and curly-I forms of an E. coli flagellum 14. We include the experimentally unobserved left-handed coiled form that is intermediate in κ and τ between the normal and semicoiled forms and thus also in Ω -space ³⁹. The first term in Eq. (4) implies that for any rotational strain $\Omega(s)$ at a given point s on the flagellum, the elastic free energy density is chosen to be that of the polymorphic form with the lowest energy. The second term in Eq. (4) enforces a smooth transition region of width ξ between two polymorphic domains.

For an E. coli flagellum, we use $A = 5.5 \,\mathrm{pN}\mu\mathrm{m}^2$ and C =3.5 pN μ m^{2 18}. The stable ground states $\Omega^{(n)} \equiv \{\Omega_1^{(n)}, \Omega_2^{(n)}, \Omega_3^{(n)}\}$ for the normal, coiled, semicoiled, and curly-I forms are, respectively (in μm^{-1}): {0.00, 1.30, -2.11}, {-0.51, 1.74, -0.56}, $\{-1.18, 1.84, 0.98\}$, and $\{-1.80, 1.56, 2.53\}^{14}$.

The ground state energies δ_n in Eq. (4) are not known yet. Their relative values determine both the height and shape of transition barriers between consecutive minima [Fig. 1(a)]. The positions $\Omega^{(n)}$ of the minima of $f_{\rm EK}$ are already fixed, as are the parabolic shapes in the neighborhood of those minima. Hence, the full landscape of the extended Kirchhoff energy density is known once the ground state energies δ_n or equivalently the transition barriers are specified.

3.1 Dynamics of the flagella

3.1.1 Equations of motion

We consider the dynamics of an elongated cell body with a flagellum emanating from an arbitrary point on its surface and moving in an unbounded fluid of viscosity η . The equations of motion of the flagellum are given by the Langevin equations for the dynamics of the centerline $\mathbf{r}(s,t)$ and the twist angle $\phi(s,t)$ about the centerline 45:

$$\partial_t \mathbf{r} = \mu_t (\mathbf{F}_{el} + \mathbf{F}_{s} + \mathbf{F}_{th}) + \mathbf{v}_h,$$
 (5)

$$\partial_t \phi = \mu_r (T_{\rm el} + T_{\rm th}). \tag{6}$$

Here the **F**'s and T's are, respectively, the local forces and torques acting on the flagellum due to elastic deformations, steric interactions, and thermal noise. We will describe them below. They are connected to the linear $(\partial_t \mathbf{r})$ and angular $(\partial_t \phi)$ velocities by the respective self-mobilities $\mu_t = \mathbf{e}_3 \otimes \mathbf{e}_3/\gamma_{\parallel} + (\mathbf{I} - \mathbf{e}_3 \otimes \mathbf{e}_3)/\gamma_{\perp}$ and $\mu_r =$ $1/\gamma_R$, where $\gamma_{\parallel} = 1.6 \times 10^{-3} \, \text{pNs}/\mu \text{m}^2$, $\gamma_{\perp} = 2.8 \times 10^{-3} \, \text{pNs}/\mu \text{m}^2$ and $\gamma_R = 1.26 \times 10^{-6} \, \text{pNs}$ are the anisotropic friction coefficients per unit length for the flagellum of an E. coli 13 . Finally, \mathbf{v}_{h} describes hydrodynamic interactions between different parts of the flagellum as detailed below.

The elastic forces and torques follow from the total elastic free energy $\mathscr{F}[\mathbf{r}(s), \phi(s)]$ as:

$$\mathbf{F}_{\mathrm{el}} = -\frac{\delta \mathscr{F}}{\delta \mathbf{r}}$$
 and $T_{\mathrm{el}} = -\frac{\delta \mathscr{F}}{\delta \phi}$. (7)

Here $\mathscr{F}[\mathbf{r}(s),\phi(s)] = \int ds (f_{\rm EK} + f_{\rm st})$, where $f_{\rm EK}$ is the Kirchhoff elastic free energy density described in the previous section and $f_{\rm st} = K(\partial_s {\bf r})^2/2$ with $K = 10^3 {\rm pN}$ is a stretching free energy density introduced to prevent local stretching of the flagellum ¹⁴.

3.1.2 Discretization procedure, thermal noise, steric and hydrodynamic interactions

Before we address the other force and torque contributions in Eqs. (5) and (6), we discuss the numerical scheme to update the flagellar configuration in time. In order to discretize the Langevin equations, we consider discrete positions $\mathbf{r}_i \equiv \mathbf{r}(s_i)$ along the flagellum and assign $\{\mathbf{e}_1(i), \mathbf{e}_2(i), \mathbf{e}_3(i)\}$ to the straight segment of length h between \mathbf{r}_{i-1} and \mathbf{r}_i [see Fig. 1 (c)]. The forces now act on the discrete points, while the torques are applied to the straight segments. To find the discretized versions of \mathbf{F}_{el} and T_{el} , we discretize the derivatives in Eqs. (7) and write $\mathscr{F}=\int ds\,(f_{\rm k}+f_{\rm st})$ as a sum over the segments.

The thermal forces \mathbf{F}_{th} and torques T_{th} in Eqs. (5) and (6), respectively, are negligible for the forward propulsion of bacteria 46 but play an important role in the polymorphic transformations during reversal of the flagellum ¹³. We, therefore, include them here. As usual, they are Gaussian random numbers with zero mean and variances $\langle (F_{\rm th}^{\parallel/\perp})^2 \rangle = 2k_BT\gamma_{\parallel/\perp}/\Delta t$, where Δt is the discrete time step used in the simulation, and \parallel and \perp denote the directions along and normal to the local tangent of the flagellum, respectively. Similarly, $\langle T_{th}^2 \rangle = 2k_B T \gamma_R / \Delta t$.

The steric force \mathbf{F}_s enforces excluded-volume interactions among different parts of the flagellum. This is needed in case Equations of motion and numerical methods distant flagellar parts try to go through each other, e.g., during a strongly buckled state. We model the steric forces following Ref. 45.

> In order to model hydrodynamic interactions between different flagellar parts, we treat each discrete point \mathbf{r}_i as a sphere of diameter equal to the thickness of the flagellum. Thus, we write $\mathbf{v}_{h}(\mathbf{r}_{i}) = \sum_{i \neq i} \mu_{i,i} \mathbf{F}(\mathbf{r}_{i})$, where the summation runs over all points of the flagellum. Here μ_{ij} is the Rotne-Prager mobility matrix ⁴⁷ for spheres at \mathbf{r}_i and \mathbf{r}_j and $\mathbf{F}(\mathbf{r}_j)$ is the force acting at \mathbf{r}_j . To be consistent with the picture that the spheres are parts of the discretized flagellum, we neglect the hydrodynamic influence of their rotation 48. Furthermore, to avoid huge computational expenses, we also neglect any correlations between thermal forces Fth acting on different points, which occur due to hydrodynamic interactions.

3.2 The cell body, rotary motor, and flagellar hook

The elongated cell body is modeled as a spherocylinder of length $L_b = 2.5 \,\mu\text{m}$ and width $d_b = 0.8 \,\mu\text{m}^{35,45}$ [see Fig. 1(c)]. A flagellum with total contour length L is attached to the point \mathbf{r}_0 on the surface of the cell body. To represent a typical flagellum undergoing a reverse rotation, we choose \mathbf{r}_0 to be on the cylindrical surface. Flagella of an E. coli are distributed randomly over the entire cell body³⁵. This implies that an arbitrarily chosen flagellum is more likely to be found on the cylindrical surface that has a larger area compared to that of the spherical ends of the cell body.

A motor tripod $\{\mathbf{e}_1(0), \mathbf{e}_2(0), \mathbf{e}_3(0)\}$ is introduced at \mathbf{r}_0 , where

 $\mathbf{e}_3(0)$ coincides with the shaft of the rotary motor driving the flagellum. A motor torque $\mathbf{T}_m = T_m \mathbf{e}_3(0)$ drives the flagellum by rotating this tripod. The main part of the flagellum is coupled to the motor tripod through the Kirchhoff elastic free energy density f_k with a bending rigidity $A \to A_h = 2.0 \,\mathrm{pN}\mu\mathrm{m}^2$, and a twist rigidity $C \to C_h = 0.1 \times 10^{-2} \,\mathrm{pN}\mu\mathrm{m}^2$ 45,49. Thus, the flagellum is connected to the motor shaft through a 'hook' that acts like a universal joint with low bending and high twist rigidities 50 and allows the first flagellar segment along $\mathbf{e}_3(1)$ to be at any angle to the motor shaft and yet efficiently transferring the driving torque to the flagellum.

The cell body translates and rotates with velocities given, respectively, by

$$\mathbf{v}_b = \mu_b^t \mathbf{F}_b$$
 and $\boldsymbol{\omega}_b = \mu_b^r (\mathbf{T}_b + \mathbf{T}_m),$ (8)

where \mathbf{F}_b and \mathbf{T}_b are the net force and torque acting on the center of mass of the cell body. They result from the force $\mathbf{F}_{\rm el} + \mathbf{F}_{\rm s}$ that acts on the flagellar anchoring point. For simplicity, the mobilities μ_b^t and μ_b^r are assigned the analytically available values for a prolate spheroid of aspect ratio L_b/d_b^{51} . As in Ref. 45 the angle between $\mathbf{e}_3(0)$ and the long axis of the cell body is set to 55° to tune the ratio for the bundle-to-body rotation rates during forward propulsion, to the experimentally observed range 18 .

Finally, the excluded volume interaction between the cell body and the flagellum is again modeled as in Ref. 45.

4 Results

4.1 Effect of barrier heights: transition from semicoiled state

As pointed out earlier, since the positions of the minima of our model elastic free energy are already fixed by the polymorphic states of the flagellum, the full energy landscape is determined once the transition barriers between consecutive minima are specified. Within our model, the barriers are determined by the differences in the ground-state energies $\{\delta_1, \delta_2, \delta_3, \delta_4\}$, which we vary in the following, in order to test how the free energy landscape affects the flagellar dynamics. Since only the relative heights of the minima are important, we set $\delta_1 = 0$.

As a starting point for a systematic study, we investigate a single transition barrier connecting two consecutive minima. In *E. coli* a typical transition between two neighboring polymorphic forms occurs between the semicoiled and curly-I state. So, we take $\delta_2 = \delta_3 = 0$ and vary δ_4 . We start with the flagellum entirely in the semicoiled form (minimum 3) and apply a motor torque in the CW sense (as viewed from outside the cell) for a duration comparable to the average tumbling time of $\sim 1 \, \text{s}$. The magnitude of the torque is fixed to a constant value of $T_m = -3.0 \, \text{pN} \mu \text{m}$, in agreement with experimental values ³⁵. A typical snapshot from our simulations for this case is shown in Fig. 1(d) (bottom).

Our observations on the nature of the semicoiled-to-curly-I transition and the stability of the curly-I form are summarized in Fig. 2. In graph (a) we plot the fraction of the flagellum in the curly-I state, $L^{\rm curly}/L$, versus time t. Below $\delta_4=0.4\,\rm pN$ the flagellum always transforms to the curly-I form, since a nonzero $L^{\rm curly}$ eventually appears as time progresses. Stability of the curly-I state increases with decreasing δ_4 and, ultimately, for $\delta_4<0.1\,\rm pN$, after an initial rapid build-up, $L^{\rm curly}$ remains close to its maximum

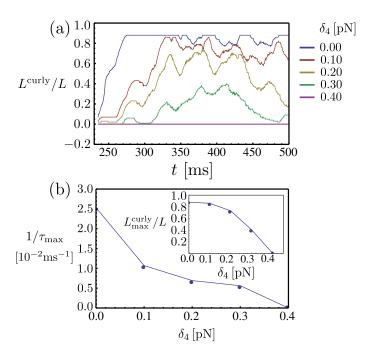


Fig. 2 Transition from semicoiled to curly-I form studied for different ground-state energies δ_4 (in pN) and $\delta_1=\delta_2=\delta_3=0.0\,\mathrm{pN}$. (a) Time evolution of the fraction of the flagellum in the curly-I state, L^curly/L . (b) Transition rate $1/\tau_\mathrm{max}$ plotted versus δ_4 , where τ_max is the time to achieve maximum length $L^\mathrm{curly}_\mathrm{max}$ in the curly-I state. Inset: $L^\mathrm{curly}_\mathrm{max}/L$ as a function of δ_4 .

value as long as the flagellum is reversely rotated. However, for $\delta_4>0.1\,\mathrm{pN}$ (and $<0.4\,\mathrm{pN}$) fluctuations in L^{curly} are huge.

These fluctuations are due to flagellar portions in the curly-I form transforming back to the semicoiled state. As δ_4 increases, the barrier height for the return jump from curly-I to semicoiled decreases and local elastic stresses built up on the curly-I portion are sufficient to induce the return transition. We find the localized elastic stresses to be due to the enhanced buckling of the curly-I form. The clockwise rotated curly-I state with its right-handed helical structure generates a thrust force towards the tumbling cell body, which is hardly translating. Thus the highly flexible curly-I form buckles more easily and produces localized elastic stresses.

Varying δ_4 also affects the maximum length $L_{\rm max}^{\rm curly}$ of curly-I form, attained along the flagellum during each run, and the transition time $\tau_{\rm max}$ to reach $L_{\rm max}^{\rm curly}$. A continuous increase in the length $L_{\rm max}^{\rm curly}$ is observed, when δ_4 decreases below the threshold value 0.4 pN [inset, Fig. 2(b)]. This resembles the behavior of an order parameter characterizing a continuous phase transition. Furthermore, the transition time $\tau_{\rm max}$ increases or the transition rate $1/\tau_{\rm max}$ decreases with growing δ_4 , indicating a slowed-down transition to the curly-I form with maximum length [Fig. 2(b)].

4.2 Effect of barrier heights: transition from normal state

Having established the importance of changing the height of one transition barrier, we now turn to the more complex problem, which is to test the dynamics of the flagellum under reverse rotation starting from the normal state. Now all three transition

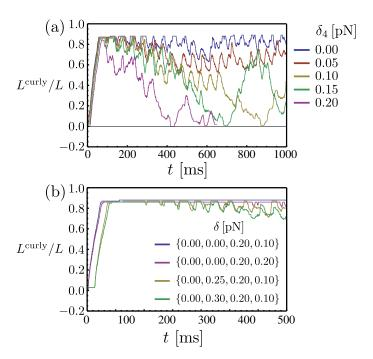


Fig. 3 Transition from the normal form under reverse rotation. (a) Time evolution of the fraction of the flagellum in the curly-I state, $L^{\rm curly}/L$, for various values of δ_4 (in pN) and $\delta_1=\delta_2=\delta_3=0.0\,{\rm pN}$. (b) $L^{\rm curly}/L$ plotted against time for selected values of δ_2 , δ_3 and δ_4 .

barriers, i.e., all three ground state energies δ_2 , δ_3 , and δ_4 become relevant. We vary them systematically as explained below. We start with a flagellum entirely in the normal form and apply a motor torque, $T_m = -3.0 \, \mathrm{pN} \mu \mathrm{m}$, in the CW sense for a time similar to the average tumbling duration. In the following, we first summarize the nature of the transition and the stability of different states and then discuss distinct dynamic phases that emerge out of our observation.

4.2.1 Nature of transition and stability

First we set $\delta_2 = \delta_3 = 0\,\mathrm{pN}$ and observe the time evolution of L^{curly}/L as we vary δ_4 [Fig. 3(a)]. We find that L^{curly} begins to increases from $t = 0\,\mathrm{ms}$ and reaches its maximum very early for each δ_4 . This implies that the flagellum directly transforms into the curly-I state without residing in a full-length semicoiled state as observed for real bacteria. Moreover, the final curly-I state is highly unstable against fluctuations for any non-zero δ_4 .

We find that these fluctuations in L^{curly} can be greatly reduced, when δ_3 is also shifted up [blue and violet curve, Fig. 3(b)]. This becomes evident when comparing the corresponding curves of Fig. 3(a) and Fig. 3(b) for the same values of δ_4 but with $\delta_3 = 0\,\text{pN}$ and $\delta_3 = 0.2\,\text{pN}$, respectively. As explained in the previous section, an increase in δ_4 reduces the barrier height for leaving the curly-I state. A simultaneous increase in δ_3 , however, restores the barrier height and thereby stabilizes the final curly-I form.

All curves in Fig. 3(a) and Fig. 3(b) (with $\delta_2=0$) attain approximately the same maximum value at nearly the same time. Moreover, for δ_3 or $\delta_4>0.35\,\mathrm{pN}$ a transition to the curly-I state does not occur at all [see Fig. 5(b)]. This implies that $L_{\mathrm{max}}^{\mathrm{curly}}$ jumps from zero to a non-zero value at the threshold $\delta_3\approx\delta_4>0.35\,\mathrm{pN}$.

Similarly, $\tau_{\rm max}$ also remains nearly constant during the transition from the normal to the curly-I state. This behavior is unlike the transition from the semicoiled to the curly-I state, where both $L_{\rm max}^{\rm curly}$ and $\tau_{\rm max}^{-1}$ continuously decrease to zero when increasing δ_4 to 0.4 pN [see Fig. 2 (b)]. Note while the semicoiled and curly-I states are separated by a single barrier, the flagellum has to be pass three barriers during the transition from the normal to the curly-I state. This might explain the discontinuous transition.

Next, we examine the effect of non-zero values of δ_2 . A comparison of the time evolution of $L^{\operatorname{curly}}/L$ for the same set of δ_3, δ_4 values but with different values of δ_2 is shown in Fig. 3(b) (yellow and green curves). It is clear that a non-zero but small value of δ_2 does not affect the above results qualitatively. The nature of the transition from the normal form and the stability of the curly-I state remain the same as before as long as δ_2 is small.

This shows that in our quest of identifying the influence of the free energy landscape on the polymorphic transformation, the most important parameters to study are δ_3 and δ_4 . In the following we therefore ignore any variation in δ_2 .

4.2.2 Dynamic states exhibited by a flagellum under reverse rotation

According to our findings, we take $\delta_2 = \delta_1 = 0$ and explore the dynamic behavior of the flagellum as we vary δ_3 and δ_4 . After a thorough examination, six distinct dynamic states emerged, which are listed in Fig. 4 in panels I-VI, respectively. Each panel plots for specific values of δ_3 and δ_4 the color-coded polymorphic forms spread along the flagellum as the flagellum evolves in time t. The distinct dynamic states are characterized as follows.

- (I) Direct transition from normal to curly-I state, which nearly spreads along the whole flagellum and is dynamically very stable.
- (II) Transition to a dynamically stable curly-I state, which is accompanied by small transient regions of semicoiled form, which appear and disappear locally.
- (III) Transition to a dynamically stable curly-I state with large transient regions of semicoiled form. The semicoiled domains appear repeatedly over time near the cell body (s=0) and move towards the free end of the flagellum, where they shed off.
- (IV) An initial nearly full-length transition to the curly-I state, followed by a reverse transition to a full-length, relatively stable semicoiled state.
- (V) Transition to a dynamically stable semicoiled form, the curly-I state is not reached.
- (VI) Dynamically stable normal form. No significant flagellar portion transforms to other polymorphic forms.

4.2.3 Energy landscape and state diagram

Combining information obtained from a range of values for δ_3 and δ_4 , we finally arrive at a comprehensive picture of the flagellar dynamics under reversal. Figure 5(a) shows how the average length $\langle L^{\text{other}} \rangle$ of the flagellar portion, which is not in the curly-I state, varies in the δ_3 - δ_4 plane. Here $\langle \cdots \rangle$ represents an average over time excluding the initial period of transition from the normal form. So, a low value of $\langle L^{\text{other}} \rangle$ implies a dynamically stable curly-I state, whereas a high value implies either large fluctuations in the curl-I state or no transition to this state. We already

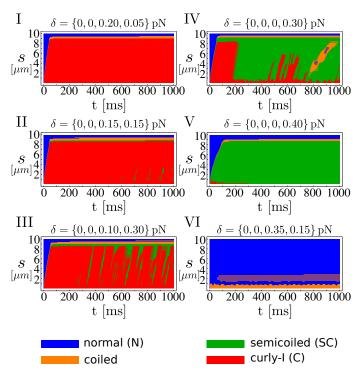


Fig. 4 Distinct dynamical states exhibited by a flagellum under reverse rotation starting from the normal state. Panels I-VI show how the polymorphic forms indicated by different colors evolve in time along the flagellum. Arclength s gives the position on the flagellum. For $\delta_1=\delta_2=0$, typically observed dynamic states are: (I) dynamically stable C state, (II) stable C state with transient SC regions, (III) repeated emergence of large transient SC regions, (IV) reverse transition from curly-I to a full-length, relatively stable SC state, (V) stable SC state, and (VI) stable N state. See text for a detailed description.

recognize that the curly-I state is unstable for high values of both δ_3 and δ_4 . However, more interestingly, we also notice that a very stable curly-I state occurs even for higher values of δ_4 provided we increase δ_3 accordingly.

Going into depth, we now monitor the detailed time evolution of the polymorphic states along the whole flagellum (like in Fig. 4) for the complete δ_3 - δ_4 plane. We identify all the dynamic states listed in the previous section and find that states I-VI are characterized by values of $\langle L^{\text{other}} \rangle$ in the ranges 0-11%, 11-15%, 15-90% and > 90% of the flagellar length. The respective regions in the δ_3 - δ_4 plane are extracted from Fig. 5(a) and represented by colors in Fig. 5(b). The corresponding dynamic states are indicated by their Roman numbers. Note that states III and IV are not distinguishable from each other by the range defined for $\langle L^{\text{other}} \rangle$. The same holds for states V and VI. However, the full time evolution of the polymorphic forms along the flagellum clearly identifies them as separate states and we mark their occurrence in the δ_3 - δ_4 plane.

5 Discussion

A comparison of our findings with experimental results should, in principle, give the unknown parameters of our extended Kirchhoff free energy. It should also reveal how accurately the elastic properties of the flagellum are described by this energy.

The relevance of our findings becomes clear, when we consider

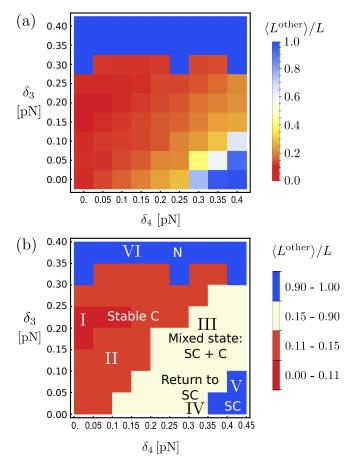


Fig. 5 Dynamic stability of curly-I state and state diagram for $\delta_1=\delta_2=0\,\mathrm{pN}.$ (a) Mean length of the flagellar portion, which is not in the curly-I form, $\langle L^{\mathrm{other}} \rangle / L$, represented in the δ_3 - δ_4 plane by a color code. (b) Colored regions in the δ_3 - δ_4 plane represent different length ranges of $\langle L^{\mathrm{other}} \rangle$ in units of the total flagellar length; dark red: 0-11%, light red: 11-15%, beige: 15-90%, and blue: > 90%. Roman numbers indicate the distinct dynamic phases shown in Fig. 4.

the full time evolution of a flagellum under reversal of the driving torque as observed in experiments ^{2,18}. For a real *E. coli*, a reversely rotated flagellum first transforms in full length to the semicoiled form, followed by the curly-I form, which persists until the rotation switches back to the CCW sense. Even though the appearance of the semicoiled domain is brief, it extends over the full flagellum and does not fluctuate into other forms until the curly-I domain grows from the cell body and takes over the whole flagellum. So, to model the flagellar dynamics under reversal correctly, the intermediate full-length semicoiled state should occur.

However, we do not observe such a behavior in the dynamic states reported in Fig. 4. The flagellum either transforms directly into the curly-I form [regions I and II in Fig. 5(b)] or it remains in the semicoiled state [region V in Fig. 5(b)]. Thus, for any combination of δ_3 and δ_4 there is never an intermediate transition to the full-length semicoiled state followed by an automatic transition to the curly-I form. This result of our model clearly is in contrast to what is often observed for real bacteria. Non-zero but small values of δ_2 should not change this behavior because, as we have shown earlier, δ_2 does not affect the dynamics in any

significant way.

One possible reason for this discrepancy with experiments is the harmonic approximation of the Kirchhoff free energy in the deformation $d\Omega$. For large deformations anharmonic terms become important. Inclusion of higher powers of $d\Omega$ in the Kirchhoff free energy would result in a highly non-trivial energy landscape, which is expected to modify the flagellar dynamics observed in our present study. Possible reasons for inclusion of extra terms might also be related to the finer details of the molecular structure of the flagellum and the hook, not investigated fully so far. Effects of such extra terms in the Kirchhoff free energy, allowed by symmetries, will be examined in the future.

An alternative way to capture the experimental pathway of the observed polymorphic transitions in E. coli within the present model is the following. There could be an internal switch, realized by some biological mechanism, that causes an effective jump in the δ_3 - δ_4 plane during the dynamics. Thus, the free energy in the first period of the flagellar reversal corresponds to the region V of Fig. 5(b), until the transformation to the semicoiled form is complete. Then, the values of δ_3 , δ_4 switch to the region I+II for the remaining part of the dynamics as long as the reversal continues.

6 Conclusions

In conclusion, we examined the dynamics of a reversely rotated *E. coli* flagellum attached to a moving cell body by thoroughly exploring the elastic free energy landscape of the flagellum. We considered a general form of the extended Kirchhoff free energy that was shown to be most appropriate for both stretching and rotation-induced polymorphism. Minima of this free energy correspond to the known polymorphic forms of the flagellum. However, the relative values of the ground state energies of those minima are not known.

We systematically studied how changes in the ground state energies influence the transition of a flagellum in two cases: from a semicoiled to the curly-I state, and from a normal to the curly-I state, respectively. These transitions are relevant during flagellar reversal.

We find that under reverse rotation, a normal flagellum can transform to a curly-I state, whose stability depends sensitively on the relative ground state energies of the involved polymorphic forms. The transition to the curly-I form can even be forbidden, making the flagellum either to continue in the normal form or to transform to a stable semicoiled state. We have classified these distinct dynamical states and obtained a state diagram for varying ground state energies. From this, one infers that for any combination of the ground state energies in our model, an intermediate transition to a full-length semicoiled state followed by a transition to the final curly-I form cannot be realized. However, we suggest an alternative way to reproduce within our model such a sequence of transitions observed for a real bacterium.

Our study provides a complete picture of how the elastic free energy landscape determines the dynamics of a reversely rotated flagellum attached to a movable cell body. Therefore, our findings are important for the proper modeling of the locomotion of a bacterium including its tumbling. We show that the full phenomenology of an E. coli flagellum cannot be realized by simply adjusting the parameters of the extended Kirchhoff free energy. This calls for alternative approaches. On the one hand, investigating the importance of anharmonic terms in the free energy or how finer details of the hook 52 influence the flageller dynamics could be two possibilities in this direction.

On the other hand, based on the established state diagram we suggested an ad hoc method to realize the correct polymorphic sequence of an *E. coli* flagellum. Implementing this method allows a thorough theoretical investigation of the complex and still not fully understood tumbling event of an *E. coli*. Moreover, since the elastic properties of bacterial flagella are similar, our method can also be applied to explore the sequence of polymorphic forms seen in other peritrichous bacteria during tumbling.

Acknowledgement

We thank the VW foundation for financial support within the program "Computational Soft Matter and Biophysics" (Grant No. 86 801)

References

- 1 S. M. Block, D. F. Blair and H. C. Berg, *Nature*, 1989, **338**, 514.
- 2 L. Turner, W. S. Ryu and H. C. Berg, J. Bacteriol., 2000, 182, 2793–2801.
- 3 N. C. Darnton and H. C. Berg, *Biophys. J.*, 2007, **92**, 2230–2236.
- 4 F. A. Samatey, K. Imada, S. Nagashima, F. Vonderviszt, T. Kumasaka, M. Yamamoto and K. Namba, *Nature*, 2001, **410**, 331–337.
- 5 S. Maki-Yonekura, K. Yonekura and K. Namba, *Nature structural & molecular biology*, 2010, **17**, 417–422.
- 6 R. E. Goldstein, A. Goriely, G. Huber and C. W. Wolgemuth, *Phys. Rev. Lett.*, 2000, **84**, 1631–1634.
- 7 D. Coombs, G. Huber, J. O. Kessler and R. E. Goldstein, *Phys. Rev. Lett.*, 2002, **89**, 118102.
- 8 H. Wada and R. R. Netz, Europhys. Lett., 2008, 82, 28001.
- 9 S. E. Spagnolie and E. Lauga, Phys. Rev. Lett., 2011, 106, 058103.
- 10 E. Lauga, Annu. Rev. Fluid Mech., 2016, 48, 105-130.
- 11 M. Kim, J. C. Bird, A. J. Van Parys, K. S. Breuer and T. R. Powers, *Proc. Natl. Acad. Sci.*, 2003, **100**, 15481–15485.
- 12 Vogel, R. and Stark, H., Eur. Phys. J. E, 2010, 33, 259-271.
- 13 R. Vogel and H. Stark, Eur. Phys. J. E, 2012, 35, 15.
- 14 R. Vogel and H. Stark, Phys. Rev. Lett., 2013, 110, 158104.
- S. Y. Reigh, R. G. Winkler and G. Gompper, *Soft Matter*, 2012, 8, 4363–4372.
- 16 M. K. Jawed, N. K. Khouri, F. Da, E. Grinspun and P. M. Reis, Phys. Rev. Lett., 2015, 115, 168101.
- 17 R. M. Macnab and M. K. Ornston, *J. Mol. Biol.*, 1977, **112**, 1 30.
- 18 N. C. Darnton, L. Turner, S. Rojevsky and H. C. Berg, *J. Bacteriol.*, 2007, **189**, 1756–1764.
- 19 M. Kong, Y. Wu, G. Li and R. G. Larson, Soft Matter, 2015, 11,

- 1572-1581.
- 20 M. Ramia, D. Tullock and N. Phan-Thien, *Biophys. J.*, 1993, **65**, 755 778.
- 21 E. Lauga and T. R. Powers, Rep. Prog. Phys., 2009, 72, 096601.
- 22 R. Cortez, L. Fauci and A. Medovikov, *Phys. Fluids*, 2005, 17, 031504.
- 23 H. Flores, E. Lobaton, S. Méndez-Diez, S. Tlupova and R. Cortez, *Bull. Math. Biol.*, 2005, **67**, 137–168.
- 24 J. Saragosti, V. Calvez, N. Bournaveas, B. Perthame, A. Buguin and P. Silberzan, *Proc. Natl. Acad. Sci.*, 2011, **108**, 16235–16240.
- 25 B. Rodenborn, C.-H. Chen, H. L. Swinney, B. Liu and H. P. Zhang, *Proc. Natl. Acad. Sci.*, 2013, **110**, E338–E347.
- 26 S. P. Strong, B. Freedman, W. Bialek and R. Koberle, *Phys. Rev. E*, 1998, **57**, 4604–4617.
- 27 D. Alizadehrad, T. Krüger, M. Engstler and H. Stark, *PLoS Comput. Biol.*, 2015, **11**, 1–13.
- 28 H. C. Fu, T. R. Powers, R. Stocker *et al.*, *Proc. Natl. Acad. Sci.*, 2012, **109**, 4780–4785.
- J. Hu, A. Wysocki, R. Winkler and G. Gompper, Sc. Rep., 2015,
 5, 9586.
- 30 S. Zhou, A. Sokolov, O. D. Lavrentovich and I. S. Aranson, *Proc. Natl. Acad. Sci.*, 2013, **111**, 1265–1270.
- 31 H. H. Wensink, J. Dunkel, S. Heidenreich, K. Drescher, R. E. Goldstein, H. Löwen and J. M. Yeomans, *Proc. Natl. Acad. Sci.*, 2012, **109**, 14308–14313.
- 32 J. Dunkel, S. Heidenreich, K. Drescher, H. H. Wensink, M. Bär and R. E. Goldstein, *Phys. Rev. Lett.*, 2013, **110**, 228102.
- 33 H. M. López, J. Gachelin, C. Douarche, H. Auradou and E. Clé-

- ment, Phys. Rev. Lett., 2015, 115, 028301.
- 34 H. Hotani, J. Mol. Biol., 1982, 156, 791 806.
- 35 H. Berg, E. coli in Motion, Springer, New York, 2004.
- 36 S. Asakura, Adv. Biophys., 1969, 1, 99-155.
- 37 C. Calldine, J. Mol. Biol., 1978, 118, 457-479.
- 38 C. Calladine, Nature, 1975, 255, 121-124.
- 39 C. Calladine, J. Theoret. Biol, 1976, 57, 469 489.
- 40 B. Friedrich, J. Math. Biol., 2006, 53, 162-178.
- 41 C. Speier, R. Vogel and H. Stark, Phys. Biol., 2011, 8, 046009.
- 42 S. V. Srigiriraju and T. R. Powers, *Phys. Rev. Lett.*, 2005, **94**, 248101.
- 43 H. Wada and R. R. Netz, Phys. Rev. Lett., 2007, 99, 108102.
- 44 L. D. Landau and E. M. Lifshitz, *Theory of Elasticity*, Pergamon, New York, 1986.
- 45 T. C. Adhyapak and H. Stark, Phys. Rev. E, 2015, 92, 052701.
- 46 P. J. A. Janssen and M. D. Graham, *Phys. Rev. E*, 2011, **84**, 011910.
- 47 J. Dhont, *An Introduction to Dynamics of Colloids*, Elsevier Science B.V, Amsterdam, 1996.
- 48 M. Reichert, PhD thesis, Universität Konstanz, 2006.
- 49 A. Sen, R. K. Nandy and A. N. Ghosh, *J. Elect. Microsc.*, 2004, **53**, 305.
- 50 K. Namba and F. Vonderviszt, Q. Rev. Biophys., 1997, 30, 1-65
- 51 S. Kim and S. Karilla, *Microhydrodynamics: Principles and Selected Applications*, Dover Publications, New York, 2005.
- 52 K. Son, J. S. Guasto and R. Stocker, *Nature physics*, 2013, 9, 494–498.